Journal of Computer and Communications, 2024, 12, 14-31
https://www.scirp.org/journal/jcc
ISSN Online: 2327-5227
ISSN Print: 2327-5219

Estimating High-Order Functional Connectivity Networks for Mild Cognitive Impairment Identification Based on Topological Structure

Guangyi Zhang, Kunpeng Zhang, Mengxue Pang*

School of Mathematics Science, Liaocheng University, Liaocheng, China
Email: *pangmengxue_lemon@163.com

How to cite this paper: Zhang, G.Y., Zhang, K.P. and Pang, M.X. (2024) Estimating High-Order Functional Connectivity Networks for Mild Cognitive Impairment Identification Based on Topological Structure. *Journal of Computer and Communications*, **12**, 14-31.
https://doi.org/10.4236/jcc.2024.123002

Received: February 10, 2024
Accepted: March 8, 2024
Published: March 11, 2024

Abstract

Functional connectivity networks (FCNs) are important in the diagnosis of neurological diseases and the understanding of brain tissue patterns. Recently, many methods, such as Pearson's correlation (PC), Sparse representation (SR), and Sparse low-rank representation have been proposed to estimate FCNs. Despite their popularity, they only capture the low-order connections of the brain regions, failing to encode more complex relationships (*i.e.*, high-order relationships). Although researchers have proposed high-order methods, like PC + PC and SR + SR, aiming to build FCNs that can reflect more real state of the brain. However, such methods only consider the relationships between brain regions during the FCN construction process, neglecting the potential shared topological structure information between FCNs of different subjects. In addition, the low-order relationships are always neglected during the construction of high-order FCNs. To address these issues, in this paper we proposed a novel method, namely Ho-FCN$_{\text{Tops}}$, towards estimating high-order FCNs based on brain topological structure. Specifically, inspired by the Group-constrained sparse representation (GSR), we first introduced a prior assumption that all subjects share the same topological structure in the construction of the low-order FCNs. Subsequently, we employed the Correlation-reserved embedding (COPE) to eliminate noise and redundancy from the low-order FCNs. Meanwhile, we retained the original low-order relationships during the embedding process to obtain new node representations. Finally, we utilized the SR method on the obtained new node representations to construct the Ho-FCN$_{\text{Tops}}$ required for disease identification. To validate the effectiveness of the proposed method, experiments were conducted on 137 subjects from the Alzheimer's Disease Neuroimaging Initiative (ADNI) database to identify Mild Cognitive Impairment (MCI) patients from the normal controls. The experimental results demonstrate superior performance compared to baseline methods.

Keywords

Ho-FCN, Sparse Representation, Mild Cognitive Impairment, Disease Recognition

1. Introduction

Resting state functional magnetic resonance imaging (rs-fMRI) is an imaging technique used to study brain function by measuring the level of neural activity in the resting state. It employs magnetic resonance imaging to observe changes in the blood oxygen level-dependent (BOLD) signal, revealing patterns of synchronization and connectivity between different brain regions. In the field of medicine, rs-fMRI finds extensive applications such as researching brain networks, neuropsychiatric disorders, individual differences, and assessing brain injuries. It holds significant clinical and research value in understanding brain diseases and the working mechanisms of the brain [1] [2].

Functional connectivity networks (FCNs) refer to networks formed by the interconnections between different regions of interest (ROIs) within the brain. These connections represent interactions and information transfer between different ROIs. FCNs based on rs-fMRI can help enhance our understanding of brain function and have been widely used in the research of various neuropsychiatric disorders, such as major depressive disorder [3] [4], attention-deficit/hyperactivity disorder [5], depression [6], Alzheimer's disease [7] [8], and more.

Up to now, researchers have proposed various effective methods for estimating FCNs, including Pearson correlation (PC) [9], sparse low-rank representation, group sparsity representation (GSR) [10], and higher-order correlations. Among them, PC is the most widely applied and effective method for FCN estimation [11]. It has advantages such as simplicity, intuitiveness, ease of computation, and understanding, making it particularly suitable for initial analysis of FCNs. However, when dealing with complex, nonlinear connectivity relationships, researchers may need to consider using more advanced methods to comprehensively estimate FCNs. PC does not fully account for confounding effects introduced by other ROIs, leading to the emergence of more reliable partial correlation estimation methods. These methods address the confounding effects through regression. Meanwhile, this introduces new challenges, as partial correlation methods require the computation of the inverse covariance matrix. Particularly in cases with numerous sample feature dimensions and a small number of subject samples, this process may face ill-conditioning issues. To ensure the reliability of the model, researchers have further introduced regularization techniques on top of partial correlation, resulting in sparse representation (SR) [12] and sparse inverse covariance estimation (SICE) [13], among other FCN estimation methods.

Although the mentioned methods provide a comprehensive estimation of FCNs, from another perspective, these methods sequentially estimate FCNs for

individual subjects. This leads to the oversight of the similarity in brain topology among different subjects. Consequently, it fails to fully capture all the information contained in the BOLD signals, potentially impacting subsequent classification performance. To address this limitation, Wee *et al.* proposed incorporating the $L_{2,1}$-norm regularization term into the FCN estimation model [10]. This introduces similarity in the topology and sparsity characteristics among different subjects. In addition, these methods only estimate low-order relationships between different ROIs, failing to capture higher-order interactions between ROIs. Researchers have introduced methods capable of extracting higher-order information for FCN estimation. For instance, Zhang *et al.* proposed a method for constructing high-order FCNs through dual correlation [14]. Wang *et al.* introduced a sparse learning-based method for constructing high-order dynamic FCNs, extracting high-order temporal features for brain disease classification [15]. Zhao *et al.* presented a clustering-based multi-view high-order FCN (Ho-FCN) framework for the diagnosis of Autism Spectrum Disorder (ASD) [16]. It's worth noting that some studies suggest that increasing the number of correlation operations may not necessarily enhance the discriminative power of the estimated FCNs. Therefore, the focus of this research primarily revolves around performing only two correlation operations for FCN estimation [17].

To address the aforementioned issues, we propose a novel method for estimating FCNs. Given our intention to incorporate potential shared topological structures among subjects during the estimation of FCNs, we initially employ the GSR method to perform a preliminary estimation of FCNs using BOLD signals, resulting in primary FCNs. This stage ensures that all subjects exhibit similarity and sparsity in the topological structure of brain networks. Although the preliminary estimated FCNs can be directly utilized for disease identification, they still contain low-order relationships from original node features and some potential noise. Therefore, we further process them by re-encoding low-order FCNs using Correlation-Preserving Embedding (COPE) [18]. This step aims to eliminate noise in low-order FCNs while preserving useful low-order relationships, yielding new node representations. Ultimately, we aim to maintain sparsity in the new node representations obtained through Correlation-Preserving Embedding. Consequently, we utilize sparse representation methods to derive the final high-order FCNs based on brain topological structure for disease classification, naming it Ho-FCN$_{\text{Tops}}$. Compared with existing methods for estimating FCNs, the proposed method has the following characteristics:

1) Proposal of a new FCN estimation method. The FCNs we estimate not only integrates low-order and high-order information to make it more comprehensive but also incorporates potential shared topological information in the brain, allowing the obtained FCNs to more accurately reflect the true state of the brain.

2) To validate the effectiveness of the proposed method, we conducted classification experiments on the ADNI dataset. The experimental results demonstrate outstanding performance of the proposed method.

The remaining sections of this paper are organized as follows. The Section 2

begins with an introduction to preprocessed data and a comprehensive review of the most pertinent studies. Subsequently, we propose a novel approach for estimating FCN, encompassing its mathematical model and algorithm. In Section 3, we describe the experimental setup and report the experimental results. In Section 4, we discuss these findings. Finally, in Section 5, we conclude this paper.

2. Materials and Methods

2.1. Data Preprocessing

The experiments in this chapter are based on the ADNI dataset, which includes 137 subjects, comprising 69 normal controls (NCs) and 68 individuals with Mild Cognitive Impairment (MCIs). The scanning parameters are as follows: the in-plane image resolution is 2.29 to 3.31 mm; slice thickness = 3.31 mm; echo time (TE) = 30 ms; repetition time (TR) is 2.2 to 3.1 s; each subject's scanning duration is 7 minutes (with a total of 140 volumes). Demographic information about the subjects can be found in Table 1, where the values represent means and standard deviations. M/F indicates male/female; MMSE stands for the Mini-Mental State Examination.

Subsequently, the subjects involved in this chapter were processed using the standard pipeline of the DPARSF (Data Processing Assistant for Resting-State fMRI) toolbox for rs-fMRI. The specific steps included: 1) removing the first three volumes from the fMRI time series of each subject to ensure signal stability; 2) performing motion correction on the remaining time series to achieve consistent slice acquisition time and mitigate the impact of head motion; specifically, subjects with frame-wise displacement (FD) greater than 0.5 mm for more than 2.5 minutes were excluded; 3) implementing nuisance regression to reduce the influence of ventricular and white matter signals. Subsequently, 4) the motion-corrected images were registered to the Montreal Neurological Institute (MNI) space, and a band-pass filter (0.015 Hz to 0.150 Hz) was applied to remove low-frequency and high-frequency noise. A spatial smoothing process with a 4 mm full-width at half-maximum (FWHM) Gaussian kernel was also applied. It is important to note that scrubbing was not performed in this chapter's experiments to avoid introducing additional artifacts. Finally, 5) using the Automated Anatomical Labeling (AAL) template, the fMRI scans' brain space was parcellated into 116 predefined ROIs through a deformable registration method, and the BOLD signals within the gray matter were extracted to calculate the average time series for each ROI.

Table 1. Demographic and clinical information of subjects in the ADNI datasets. Values are reported as mean ± standard deviation. M/F, male/female; MMSE, mini-mental examination.

Dataset	Class	Gender (M/F)	Age (years)	MMSE
ADNI	MCI	39/29	76.50 ± 13.50	26.77 ± 1.23
	NC	17/52	71.50 ± 14.50	28.82 ± 1.15

2.2. Baseline Methods for FCN Construction

2.2.1. Pearson's Correlation

As mentioned previously, PC, outlined in [19], stands as the simplest and widely adopted technique for constructing FCNs. In this approach, the correlation between distinct brain regions is established by computing Pearson's correlation coefficients based on the BOLD signals from two ROIs.

In PC-based FCNs, the edge weight w_{ij} between two ROIs is defined as follows:

$$w_{ij} = \frac{\left(x_i - \bar{x}_i\right)^{\mathrm{T}}\left(x_i - \bar{x}_i\right)}{\sqrt{\left(x_i - \bar{x}_i\right)^{\mathrm{T}}\left(x_i - \bar{x}_i\right)}\sqrt{\left(x_j - \bar{x}_j\right)^{\mathrm{T}}\left(x_j - \bar{x}_j\right)}} \tag{1}$$

where $x_i \in R^T \quad \left(i = 1, 2, \cdots, M\right)$ is the BOLD signal of the *ith* ROI. T is length of the time series and M is numbers of ROI.

Without loss of generality, we redefine $x_i = \left(x_i - \bar{x}_i\right) \Big/ \sqrt{\left(x_i - \bar{x}_i\right)^{\mathrm{T}}\left(x_i - \bar{x}_i\right)}$. Then, Equation (1) can be simplified as $w_{ij} = x_i^{\mathrm{T}} x_j$, which corresponds to the optimal solution of the following model:

$$\min_{w_{ij}} \quad \sum_{i,j}^{M} \left\| x_i - w_{ij} x_j \right\|^2 \tag{2}$$

Equation (2) can be further expressed in matrix form, whose form is:

$$\min_{W} \quad \left\| W - X^{\mathrm{T}} X \right\|_F^2, \tag{3}$$

where $X = \left[x_1, x_2, \cdots, x_M\right] \in R^{T \times M}$ is the BOLD signals matrix. Here, $W = \left(w_{ij}\right) \in R^{M \times M}$ is the FCN estimated using PC, and $\left\| \cdot \right\|_F$ represents the Frobenius-norm of a matrix.

2.2.2. Sparse Representation

Different from PC, which measures the full correlation, partial correlation estimates the functional connectivity between a pair of ROIs while considering the effects from other ROIs [20]. However, vanilla partial correlation is typically performed by calculating the inverse covariance matrix, which may result in ill-conditioned problems. To address this issue, regularization terms are introduced into the partial correlation model to obtain a more robust and reliable FCN. For example, SR encodes the sparsity of the FCN by introducing an L_1 -norm regularization term [21]. The model is defined as follows:

$$\begin{aligned} \min_{w_{ij}} \quad & \sum_{i=1}^{M} \left(\left\| x_i - \sum_{j \neq i} w_{ij} x_j \right\|^2 + \lambda \sum_{j \neq i} \left| w_{ij} \right| \right) \\ \text{s.t.} \quad & w_{ii} = 0, \forall\, i = 1, 2, \cdots, M \end{aligned} \tag{4}$$

where λ is the regularization parameter that controls the sparsity of the brain network W.

The expression provided in Equation (4) can be reformulated in the following matrix form:

$$\begin{aligned} \min_{W} \quad & \left\| X - XW \right\|_F^2 + \lambda \left\| W \right\|_1 \\ \text{s.t.} \quad & w_{ii} = 0, \forall\, i = 1, 2, \cdots, M \end{aligned} \tag{5}$$

where $\|\cdot\|_1$ denotes the L_1-norm of a matrix for modeling sparsity prior into the constructed FCN. It is important to note that the constraint $w_{ii}=0$ ensures that the diagonal elements of W are entirely zeros, preventing degenerate solutions.

2.2.3. High-Order FCN Estimation Methods

As mentioned earlier, researchers have proposed various high-order FCN estimation methods [22] [23]. However, in our study, we chose to review only functional connectivity estimation methods focusing on second-order correlations (*i.e.*, correlation's correlation). Studies indicate that estimation methods based on second-order correlations are often simple yet effective [17]. Taking the example of the high-order PC method, it initially utilizes the PC method to calculate the Pearson correlation coefficient k_{ij} for the BOLD signals corresponding to each ROI pair, thus forming low-order FCNs. Subsequently, for the obtained low-order FCNs, the Pearson correlation coefficients K_{IJ} for rows and columns are calculated in the same manner, ultimately creating high-order FCNs required for disease identification. The implementation steps of other high-order FCN estimation methods (such as SR + SR) are similar to those of the high-order PC method.

2.3. FCN Estimation via Ho-FCN$_{\text{Tops}}$

As previously mentioned, researchers have developed various methods for estimating FCNs, including some that can only simulate low-order relationships between ROIs, such as PC and SR, as well as some high-order FCNs construction methods like SR + SR and Ho-FCN$_{\text{COPE}}$. However, these methods have certain limitations. In light of this, our research motivation has two main aspects: 1) to integrate low-order and high-order information between ROIs, fully harnessing the advantages of high-order FCNs, enhancing the quality of FCN estimation, and making it more conducive to subsequent disease recognition tasks; 2) some common FCN estimation methods only utilize spatial relationships between ROIs, overlooking the potential shared topological structure among subjects. To address this issue, we propose a high-order FCN estimation method based on brain topological structure. The specific model is shown in Figure 1. The specifics of the motivation for fusing brain topologies are shown in Figure 2.

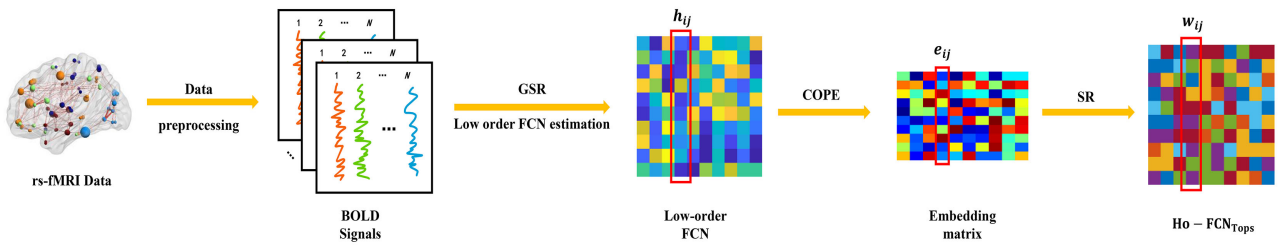

Figure 1. The pipeline of building Ho-FCN$_{\text{Tops}}$.

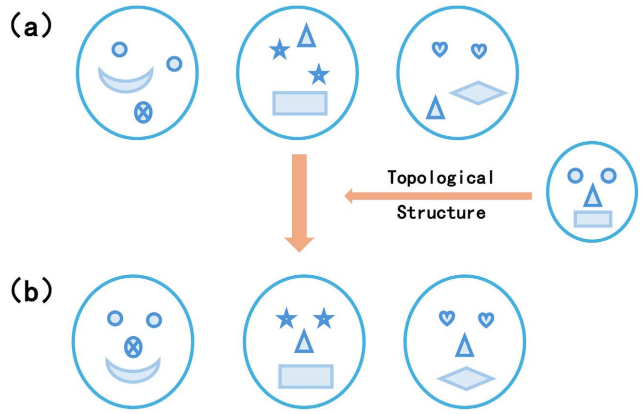

Figure 2. Elucidate our motives. We depicted three distinct cartoon faces, each corresponding to a subject's FCN. (a) The topological structure is not included. Despite the shared characteristics of the cartoon faces, there are evident variations in facial topological structures among different subjects. (b) FCNs are constructed based on a common topology. Different subjects share the same topology, resulting in similar face topologies and facial features.

Compared to the basic low-order FCN construction methods described earlier, high-order FCN construction methods can consider deeper interactions between ROIs, thereby extracting more information useful for recognition tasks. However, such methods overlook the potential topological structure among subjects. Based on this, our proposed high-order FCN estimation method, which integrates brain topological structure, comprises three main steps. Firstly, we replace the commonly used SR method in high-order FCN construction with the GSR method for the preliminary estimation of low-order FCN between different ROIs. In contrast to SR methods, GSR introduces a group-level prior, assuming that all subjects share the same topological structure. This process relies on the introduction of the $L_{2,1}$-norm, a constraint that integrates the shared topological structure into the FCN construction process, ensuring that the estimated FCN has a certain degree of sparsity [10] [24]. Calculating the low-order FCN using the GSR is represented as $H=\left(h_{ij}\right)_{p\times p}$, as shown in Equation (6).

$$\min_{H_i} \sum_{n=1}^{N}\left(\frac{1}{2}\left\|x_i^n - X_{-i}^n h_i^n\right\|_2^2\right) + \lambda_1 \left\|H_i\right\|_{2,1} \tag{6}$$

where N is the number of subjects, p is the number of ROIs and x_i^n is the BOLD signal time series of the *ith* ROI of the *nth* subject. Besides, h_i^n is the weight vector that denotes the effect of other ROIs to the *ith* ROI for the *nth* subject, and H_i is the corresponding weight matrix composed of the *ith* ROI of all N subjects. The notation $\left\|\cdot\right\|_{2,1}$ is the $L_{2,1}$-norm.

As mentioned earlier, current high-order estimation methods involve directly applying second-order correlation representations to the adjacency matrix of low-order FCN. This approach has drawbacks, as it not only introduces noise from the low-order FCN into the estimation process of the high-order FCN, af-

fecting the quality of the high-order FCN estimation, but also fails to determine whether the low-order relationships among valuable ROIs in the low-order FCN are fully preserved during the high-order FCN estimation process. Following Su *et al.*'s research [18], we employ COPE to re-encode the low-order FCN, ensuring the elimination of noise information in H while retaining the original low-order spatial relationships among ROIs in H. Specifically, the implementation of COPE involves re-encoding the obtained H. This is achieved by minimizing the following objective function to generate a new node representation $E=\left[e_1,e_2,\cdots,e_P\right]\in R^{m\times p}$, with the detailed objective function outlined in Equation (7).

$$\Psi\left(E\right)=\sum_{i=1}^{p}\left\|e_i-\sum_{j=1}^{p}h_{ij}e_j\right\|^2 \tag{7}$$

where e_i is the new node representation for node i in the low-dimensional embedding space, and h_{ij} represents the edge weights of the previously estimated low-order brain functional network in the preceding step. In Equation (7), the weights h_{ij} in the low-order brain functional network serve as the encoding of the low-order information required for the high-order FCN. Therefore, to ensure the effective preservation of low-order information, it is only necessary to find a suitable embedding space through COPE. We can apply mathematical knowledge to simplify Equation (7) into the matrix form of Equation (8) and impose constraints on $tr\left(EE^{\mathrm{T}}\right)=p$ to avoid the occurrence of trivial solutions.

$$\begin{aligned}\Psi\left(E\right)&=\sum_{i=1}^{p}\left\|EI_iEH_i\right\|^2\\&=tr\left(E\left(I-H\right)\left(I-H\right)^{\mathrm{T}}E^{\mathrm{T}}\right)\end{aligned} \tag{8}$$

Thus, we obtain the following COPE model, where $L=\left(I-H\right)\left(I-H\right)^{\mathrm{T}}$:

$$\begin{aligned}\min_{W}\quad & tr\left(ELE^{\mathrm{T}}\right)\\ \text{s.t.}\quad & tr\left(EE^{\mathrm{T}}\right)=p\end{aligned} \tag{9}$$

Ultimately, we can transform Equation (9) using the Lagrange multiplier method and then complete the optimization to find the optimal values. The solution, when expressed in matrix form, is shown in Equation (10):

$$\begin{aligned}\min_{W}\quad & \left\|E-EW\right\|_F^2+\lambda_2\left\|W\right\|_1\\ \text{s.t.}\quad & w_{ii}=0,\forall\, i=1,2,\cdots,p\end{aligned} \tag{10}$$

where λ_2 is a regularization parameter, used to control the balance between the two terms in the objective function, and w_{ij} represents the high-order correlation coefficient between the *i-th* and *j-th* ROIs in the finally obtained Ho-FCN$_{\text{Tops}}$.

3. Experiments and Results

3.1. Experimental Setting

3.1.1. Hyper-Parameters of FCN Estimates

In our experiments, we selected two classic methods, PC and SR, as baselines for

estimating FCN. Additionally, we adopted three high-order FCN estimation methods based on correlation, including the latest research advancements: SR + SR, GSR + SR, and Ho-FCN$_{COPE}$ [18]. These methods, except for PC, all involve one or more hyper-parameters. To ensure fairness, we configured different sparsity combinations for the PC method, choosing candidate parameters from 11 threshold values in the range [1%, 9%, ⋯, 89%, 99%]. Each parameter represents the percentage of weak connections to be discarded. For the hyper-parameters λ_1 and λ_2 of the other four baseline methods, we constrained their range to $[2^{-10}, 2^{-9}, \cdots, 2^{-1}, 2^{0}]$ to ensure optimal performance and consistency with state-of-the-art methods. Simultaneously, we will select hyper-parameters from the range $[2^{-6}, 2^{-5}, \cdots, 2^{-1}, 2^{0}]$ for our proposed method to ensure its robust classification performance.

3.1.2. Feature Selection and Classification

As we are aware, the field of medical imaging commonly grapples with the challenge of limited data samples, and our research is similarly affected by this issue. Our dataset comprises 137 subjects, and to validate the effectiveness of the proposed method, we employ a leave-one-out cross-validation (LOOCV) strategy. Specifically, from the pool of 137 subjects, we initially select one sample as the test set, with the remaining 136 serving as the training set. Simultaneously, these 136 subjects undergo internal LOO training and testing iterations. This process repeats iteratively until each experimental sample has completed one testing cycle. Refer to Figure 3 for the detailed selection of optimal parameter pipelines through leave-one-method cross-validation

After completing the estimation of FCNs for all subjects, the next step is to perform disease identification and classification based on the obtained FCNs. For the subject sample used in this study, each subject has 116 ROIs, corresponding to a total of $116\times(116-1)=13340$ features when calculating the correlations between these ROIs. Since the estimated FCNs are symmetric, we only need to consider the upper triangular matrix elements of the FCNs as input features for the classifier, resulting in a final feature count of $\frac{116\times(116-1)}{2}=6670$.

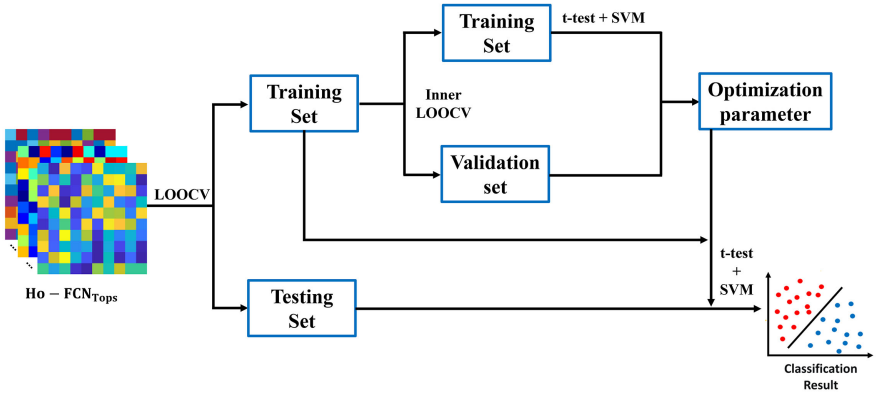

Figure 3. Selection of the optimal parameter pipeline via leave-one-out cross-validation.

It is essential to note that the number of subjects in the dataset we utilized is only 137, significantly smaller than the number of features. This situation often leads to the curse of dimensionality, potentially affecting subsequent classification performance. Although researchers have proposed various feature selection methods to address this issue, our primary objective is to evaluate the effectiveness of the proposed FCNs estimation method in disease identification [25] [26]. Therefore, in this study, we employed a simple and effective t-test method for feature selection, with a fixed $p = 0.01$ based on empirical considerations. To identify subjects with MCI from the NCs, we opted for the widely-used Support Vector Machine (SVM) classifier. Research indicates that SVM exhibits excellent performance in this context, with default parameters set at $C = 1$ [27] [28].

3.1.3. Performance Evaluation Metrics

To comprehensively assess the performance of our proposed method in terms of classification, we selected eight metrics for comparative evaluation. This aims to quantify the improvements of our method relative to the control method. The metrics include accuracy (ACC), specificity (SPE), sensitivity (SEN), F_1-score, balanced accuracy (BAC), positive predictive value (PPV) and negative predictive value (NPV). The mathematical definitions of these metrics are as follows:

$$\mathrm{ACC} = \frac{\mathrm{TP} + \mathrm{TN}}{\mathrm{TP} + \mathrm{TN} + \mathrm{FP} + \mathrm{FN}} \tag{11}$$

$$\mathrm{SEN} = \frac{\mathrm{TP}}{\mathrm{TP} + \mathrm{FN}} \tag{12}$$

$$\mathrm{SPE} = \frac{\mathrm{TN}}{\mathrm{TN} + \mathrm{FP}} \tag{13}$$

$$\mathrm{BAC} = \frac{\mathrm{SEN} + \mathrm{SPE}}{2} \tag{14}$$

$$\mathrm{PPV} = \frac{\mathrm{TP}}{\mathrm{TP} + \mathrm{FP}} \tag{15}$$

$$\mathrm{NPV} = \frac{\mathrm{TN}}{\mathrm{TN} + \mathrm{FN}} \tag{16}$$

$$\mathrm{F_1\text{-score}} = \frac{2\mathrm{TP}}{2\mathrm{TP} + \mathrm{FN} + \mathrm{FP}} \tag{17}$$

Please note that in this study, subjects with MCI are considered positive class, while NC samples are considered negative class. In which, TP, TN, FP, FN respectively represent true positive, true negative, false positive, and false negative.

3.2. Results of MCI Identification

In Table 2, we present the performance of the proposed method Ho-$\mathrm{FCN_{Tops}}$ and five other baseline methods in the MCI recognition task. The experimental results indicate that the Ho-$\mathrm{FCN_{Tops}}$ method outperforms the baseline methods on three major metrics, with primary performance indicators being ACC = 0.8905, SEN = 0.8824, and SPE = 0.8986 at $p = 0.01$. Furthermore, our method exhibits superior performance across other performance metrics. Overall, in the

Table 2. The classification performance of six methods, including Pearson's correlation (PC), Sparse Representation (SR), and high-order methods (*i.e.*, SR + SR, GSR + SR, the Ho-FCN constructed based on COPE (Ho-FCN$_{COPE}$), and the Ho-FCN constructed based on topological structure (Ho-FCN$_{Tops}$) on ADNI dataset. Seven quantitative metrics, including accuracy (ACC), specificity (SPE), sensitivity (SEN), F1-score (F1), balanced accuracy (BAC), positive predictive value (PPV), and negative predictive value (NPV) are used to evaluate the performance of these methods.

Method	ACC	SEN	SPE	F1	BAC	PPV	NPV
PC	0.8540	0.8676	0.8406	0.8551	0.8541	0.8429	0.8657
SR	0.8248	0.8088	0.8406	0.8209	0.8247	0.8333	0.8169
SR + SR	0.7372	0.7059	0.7681	0.7273	0.7370	0.7500	0.7260
GSR + SR	0.6642	0.5000	0.8261	0.5965	0.6630	0.7391	0.6264
Ho-FCN$_{COPE}$ [18]	0.8248	0.8088	0.8406	0.8209	0.8247	0.8333	0.8169
Ho-FCN$_{Tops}$	**0.8905**	**0.8824**	**0.8986**	**0.8889**	**0.8905**	**0.8955**	**0.8857**

MCI recognition task, the proposed method in this paper demonstrates better classification performance.

The conclusions drawn from Table 2 suggest that integrating topological structure into the estimation process of FCNs contributes to improving classification performance in disease recognition tasks. In the next section, we will delve into a detailed discussion of various factors and their impact on the final classification performance.

4. Discussion

4.1. Sensitivity to Embedding Dimension

The embedding dimension plays a crucial role in achieving outstanding classification performance. Therefore, in this section, to assess the impact of the embedding dimension on classification performance, we will explore the effects of different embedding dimensions on the estimation of FCNs and classification performance. Here, the embedding dimension m takes values from [40, 50, ⋯, 110], encompassing a total of 8 dimensions. As evident from Figure 4, the classification performance is highly sensitive to changes in the embedding dimension m, indicating that different embedding dimensions have varying effects on classification performance, as clearly observed in Figure 4.

Furthermore, we observed a trend in the classification performance during the transition from higher to lower embedding dimensions, showing an initial increase followed by a subsequent decrease. When $m = 80$, the classification performance reached its peak, leading in ACC, SEN, and SPE metrics compared to other embedding dimensions. However, for $m < 80$, the classification metrics exhibited varying degrees of decline. This might be attributed to excessive reduction in dimensionality, potentially resulting in a significant loss of useful information for classification, thereby affecting subsequent FCNs estimation and classification. Consequently, in the subsequent discussions, we will focus on the case where $m = 80$.

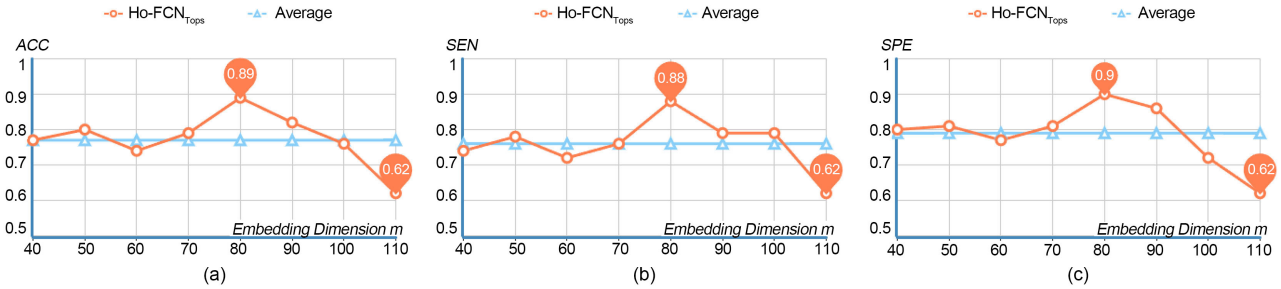

Figure 4. Evaluate the impact of embedding dimensions on classification performance. We chose to use the following disaggregated measures for assessment: (a) ACC, (b) SEN and (c) SPE. To provide a clearer depiction of the influence of embedding dimensions on classification performance, we conducted an averaging operation on the classification metrics under different embedding dimensions and presented the results for better visualization.

4.2. Sensitivity to Network Modelling Parameters

In practical classification tasks, the ultimate classification accuracy is influenced by various factors, with model parameters being a key factor, a viewpoint validated by many researchers [29] [30]. To investigate the impact of model hyper-parameters on the final classification performance, we present in **Figure 5** the classification performance under different parameter combinations for a more intuitive understanding and discussion of the results. In **Figure 5**, we observe that the optimal accuracy is achieved when $m=80$, $\lambda_1=2^{-1}$, and $\lambda_2=2^{-5}$, with ACC = 0.9343. Please note that the accuracy shown in **Figure 5** is based on the LOO strategy. Additionally, we find that as the value of hyper-parameter λ_1 approaches 2^0, the corresponding classification performance shows an upward trend. This may be attributed to the increase in λ_1 enhancing the $L_{2,1}$-norm constraint, thereby strengthening the constraint on the potential shared topological structure, contributing to improved classification performance to some extent.

Moreover, for hyper-parameter λ_2, smaller values tend to enhance classification performance. Through the analysis of the estimated FCNs, we discover that as the value of λ_2 increases, the resulting network becomes sparser, potentially leading to the discard of many useful pieces of information for classification, thereby reducing classification performance. Overall, when the hyper-parameter values are concentrated in the region above **Figure 5**, superior classification performance can be achieved.

4.3. Visualization of the FCNs

Achieving high-quality FCNs is crucial for attaining superior classification performance. Therefore, estimating high-quality FCNs becomes paramount. Visualizing the estimated FCNs helps to intuitively understand the strengths and weaknesses of different methods. It is important to note that, for a unified comparison of different methods, the adjacency matrices shown in **Figure 6** have been normalized to the interval [−1, 1]. Observations from **Figure 6** include:

1) The method based on PC presents significant differences compared to other methods. This is because the PC-based method adopts a strategy entirely different

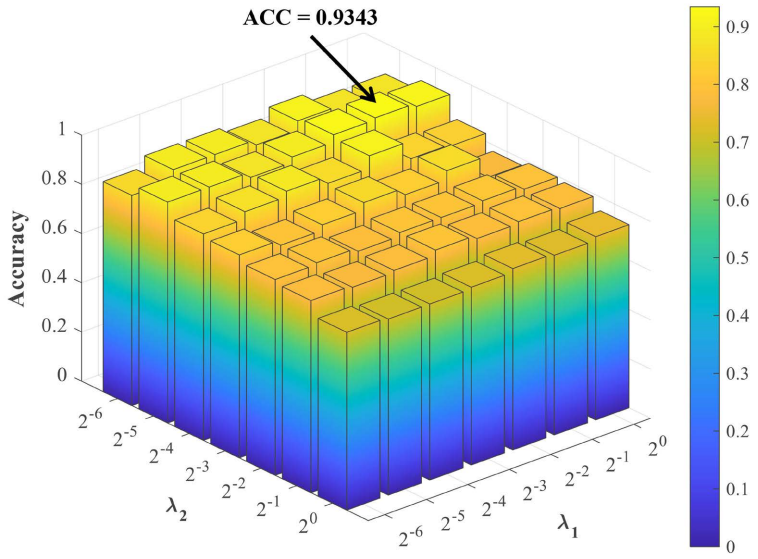

Figure 5. Classification accuracy of the networks estimated by the proposed method at different combinations of regularization parameters. The results were obtained by the LOO test for all subjects.

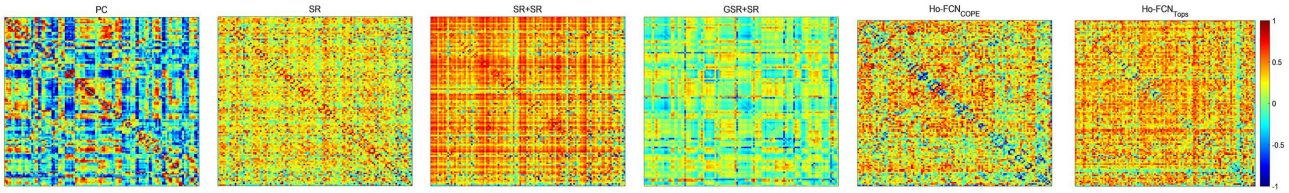

Figure 6. Network edge weight matrices for the same subject were obtained based on six different methods (PC, SR, SR + SR, GSR + SR, Ho-FCN$_{COPE}$ and the proposed Ho-FCN$_{Tops}$).

from other methods in capturing relationships between different ROIs, leading to distinct visual differences in FCN representations.

2) For the other five correlation-based methods, they all exhibit varying degrees of sparsity in the visualization of adjacency matrices due to the utilization of SR operations.

3) Our proposed Ho-FCN$_{Tops}$ method incorporates the potential shared brain topological structure compared to the Ho-FCN$_{COPE}$ method. In Figure 6, a clear line is observable in the adjacency matrices of FCNs estimated by the Ho-FCN$_{Tops}$ method for some ROIs, suggesting the integration of shared topological structure into the estimation process, which is genuinely reflected in the final FCNs. Additionally, FCNs constructed by the Ho-FCN$_{Tops}$ method appear cleaner, indicating the significant role of the potential shared topological relationships in FCN estimation.

4.4. Compared with the Previous Works

In Table 2, we show the experiment results of five previous methods (*i.e.*, PC, SR, SR + SR, GSR + SR, and Ho-FCN$_{COPE}$) and the Ho-FCN$_{Tops}$. Compared with these previous works, we have the following interesting observations. First, the

Ho-FCN$_{Tops}$ performs better than PC and SR. One possible reason is that the Ho-FCN$_{Tops}$ can capture the complex relationships, which can reflect the real state of the brain. Second, compared with SR + SR and GSR + SR, the Ho-FCN$_{Tops}$ and Ho-FCN$_{COPE}$ can achieve better performance. One possible reason is that both of the Ho-FCN$_{Tops}$ and Ho-FCN$_{COPE}$ eliminate noise and redundancy from the low-order FCNs, resulting in the constructed FCNs more clearly. In addition, we find that the Ho-FCN$_{Tops}$ performs better than Ho-FCN$_{COPE}$. The main possible reason is that the Ho-FCN$_{COPE}$ cannot encode the topological information of the brain, and in Section 4.5, we will show more details.

4.5. The Influence of Brain Topology Structure

The proposed method makes a significant contribution by integrating potential shared brain topological structures during the estimation of high-order FCNs. Therefore, a discussion regarding the impact of brain topological structures on FCNs estimation becomes imperative. By examining the classification performance presented in Table 2 and Figure 7, we can initially observe that our method outperforms five baseline methods across seven performance evaluation metrics. Notably, when compared to three other high-order FCNs construction methods that do not consider brain topological structures, particularly in comparison to Ho-FCN$_{COPE}$, our proposed method demonstrates significant advantages. This underscores that integrating potential shared brain topological structures during the estimation of high-order FCNs leads to superior classification performance.

4.6. Discriminative Features

For the estimated FCNs, they can not only be used for disease identification but also for the detection of potential biomarkers related to diseases. Through feature selection on the estimated FCNs, we can obtain ROIs with higher relevance to disease identification, thereby identifying potential biomarkers associated with MCI. Therefore, we employed a t-test with a significance level of $p = 0.0005$

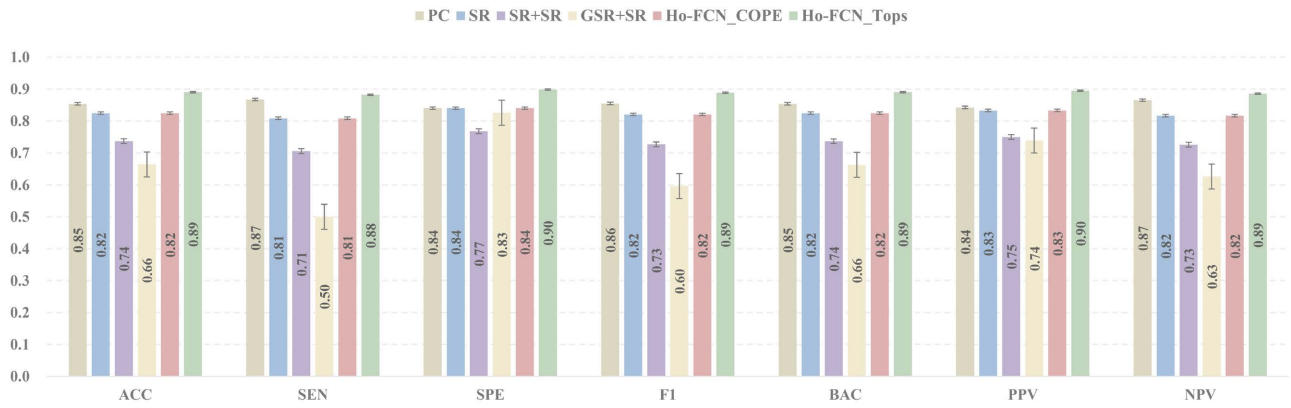

Figure 7. Classifying with six different methods across seven evaluation metrics. The horizontal axis represents the seven distinct evaluation metrics, while the vertical axis represents the average classification results.

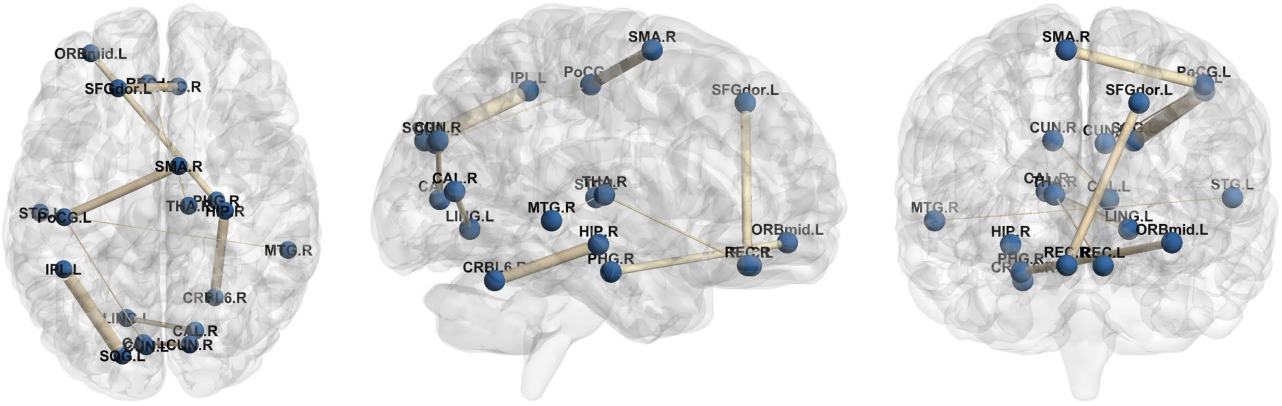

Figure 8. The discriminative features with t-test selection are identified for MCI classification. Each arc in the figure displays the selected feature between two ROIs, where the thickness indicates its discriminative power for classification.

for feature selection on the estimated FCNs. After the t-test selection, a total of 36 discriminative features were chosen. Among them, we selected the top 10 most discriminative features and visually presented them in Figure 8. From Figure 8, it can be observed that these features include the hippocampus, temporal lobe, parahippocampal gyrus, and other 10 most discriminative features. According to a review of potential neuroimaging biomarkers for MCI, these regions are closely related to the identification of MCI diseases. The application of these biomarkers can improve the specificity of clinical diagnosis and enhance the prediction of disease progression [31] [32] [33].

5. Conclusions

In this paper, we have focused on addressing several challenges in current FCN research. These challenges include overlooking the potential shared topological structure among different subjects and the difficulties in noise reduction and preservation of low-order relationships during high-order FCN construction. By introducing a novel high-order FCN estimation method based on brain topological structure, we have leveraged the information embedded in the brain's topological structure. This method integrates low-order information into the construction process of high-order FCN, presenting a novel tool for the diagnosis of MCI. In experiments conducted on the public ADNI database, we have demonstrated significant performance advantages. Compared to baseline methods, our proposed approach achieved superior results in MCI recognition tasks, confirming the effectiveness of our method.

While we have made some progress in FCN estimation, we acknowledge that there are many issues that require further exploration. Therefore, in future research, we will focus on the following aspects: 1) Extend our approach to the diagnosis of other neurological disorders, such as MDD, ASD, etc. 2) Enhance our understanding of brain topological structure and optimize FCN estimation methods accordingly. 3) Further apply machine learning methods to improve the accuracy and generalization of FCN estimation. By conducting in-depth research

in these directions, we aim to provide more comprehensive and effective solutions for the early diagnosis of neurological disorders, the development of treatment methods, and a deeper understanding of brain connectivity patterns.

Conflicts of Interest

The authors declare no conflicts of interest regarding the publication of this paper.

References

[1] Lee, M.H., Smyser, C.D. and Shimony, J.S. (2013) Resting-State fMRI: A Review of Methods and Clinical Applications. *American Journal of Neuroradiology*, **34**, 1866-1872. https://doi.org/10.3174/ajnr.A3263

[2] Canario, E., Chen, D. and Biswal, B. (2021) A Review of Resting-State fMRI and Its Use to Examine Psychiatric Disorders. *Psychoradiology*, **1**, 42-53. https://doi.org/10.1093/psyrad/kkab003

[3] Bondi, E., Maggioni, E., Brambilla, P. and Delvecchio, G. (2023) A Systematic Review on the Potential Use of Machine Learning to Classify Major Depressive Disorder from Healthy Controls Using Resting State fMRI Measures. *Neuroscience & Biobehavioral Reviews*, **144**, Article ID: 104972. https://doi.org/10.1093/psyrad/kkab003

[4] Pilmeyer, J., Huijbers, W., Lamerichs, R., Jansen, J.F., Breeuwer, M. and Zinger, S. (2022) Functional MRI in Major Depressive Disorder: A Review of Findings, Limitations, and Future Prospects. *Journal of Neuroimaging*, **32**, 582-595. https://doi.org/10.1111/jon.13011

[5] An, L., Cao, Q.-J., Sui, M.-Q., Sun, L., Zou, Q.-H., Zang, Y.-F. and Wang, Y.-F. (2013) Local Synchronization and Amplitude of the Fluctuation of Spontaneous Brain Activity in Attention-Deficit/Hyperactivity Disorder: A Resting-State fMRI Study. *Neuroscience Bulletin*, **29**, 603-613. https://doi.org/10.1007/s12264-013-1353-8

[6] Wu, Q.-Z., Li, D.-M., Kuang, W.-H., Zhang, T.-J., Lui, S., Huang, X.-Q., Chan, R.C., Kemp, G.J. and Gong, Q.-Y. (2011) Abnormal Regional Spontaneous Neural Activity in Treatment-Refractory Depression Revealed by Resting-State fMRI. *Human Brain Mapping*, **32**, 1290-1299. https://doi.org/10.1002/hbm.21108

[7] Ibrahim, B., Suppiah, S., Ibrahim, N., Mohamad, M., Hassan, H.A., Nasser, N.S. and Saripan, M.I. (2021) Diagnostic Power of Resting-State fMRI for Detection of Network Connectivity in Alzheimer's Disease and Mild Cognitive Impairment: A Systematic Review. *Human Brain Mapping*, **42**, 2941-2968. https://doi.org/10.1002/hbm.25369

[8] Agosta, F., Pievani, M., Geroldi, C., Copetti, M., Frisoni, G.B. and Filippi, M. (2012) Resting State fMRI in Alzheimer's Disease: Beyond the Default Mode Network. *Neurobiology of Aging*, **33**, 1564-1578. https://doi.org/10.1016/j.neurobiolaging.2011.06.007

[9] Smith, S.M., Vidaurre, D., Beckmann, C.F., Glasser, M.F., Jenkinson, M., Miller, K.L., Nichols, T.E., Robinson, E.C., Salimi-Khorshidi, G., Woolrich, M.W., *et al.* (2013) Functional Connectomics from Resting-State fMRI. *Trends in Cognitive Sciences*, **17**, 666-682. https://doi.org/10.1016/j.tics.2013.09.016

[10] Wee, C.-Y., Yap, P.-T., Zhang, D., Wang, L. and Shen, D. (2014) Group Constrained Sparse fMRI Connectivity Modeling for Mild Cognitive Impairment Iden-

tification. *Brain Structure and Function*, **219**, 641-656. https://doi.org/10.1007/s00429-013-0524-8

[11] Qiao, L., Zhang, L., Chen, S. and Shen, D. (2018) Data-Driven Graph Construction and Graph Learning: A Review. *Neurocomputing*, **312**, 336-351. https://doi.org/10.1016/j.neucom.2018.05.084

[12] Peng, J., Wang, P., Zhou, N. and Zhu, J. (2009) Partial Correlation Estimation by Joint Sparse Regression Models. *Journal of the American Statistical Association*, **104**, 735-746. https://doi.org/10.1198/jasa.2009.0126

[13] Sun, L., Patel, R., Liu, J., Chen, K., Wu, T., Li, J., Reiman, E. and Ye, J. (2009) Mining Brain Region Connectivity for Alzheimer's Disease Study via Sparse Inverse Covariance Estimation. *Proceedings of the* 15*th ACM SIGKDD International Conference on Knowledge Discovery and Data Mining*, Paris, 28 June-1 July 2009, 1335-1344. https://doi.org/10.1145/1557019.1557162

[14] Zhang, H., Chen, X., Shi, F., Li, G., Kim, M., Giannakopoulos, P., Haller, S. and Shen, D. (2016) Topographical Information-Based High-Order Functional Connectivity and Its Application in Abnormality Detection for Mild Cognitive Impairment. *Journal of Alzheimer's Disease*, **54**, 1095-1112. https://doi.org/10.3233/JAD-160092

[15] Wang, J., Jie, B., Zhang, X., Li, W., Wu, Z. and Yang, Y. (2023) Sparse-Learning Based High-Order Dynamic Functional Connectivity Networks for Brain Disease Classification. *Proceedings of the* 2023 7*th International Conference on Machine Learning and Soft Computing*, Chongqing, 5-7 January 2023, 161-167. https://doi.org/10.1145/3583788.3583812

[16] Zhao, F., Zhang, X., Thung, K.-H., Mao, N., Lee, S.-W. and Shen, D. (2021) Constructing Multi-View High-Order Functional Connectivity Networks for Diagnosis of Autism Spectrum Disorder. *IEEE Transactions on Biomedical Engineering*, **69**, 1237-1250. https://doi.org/10.1109/TBME.2021.3122813

[17] Guo, T., Zhang, Y., Xue, Y., Qiao, L. and Shen, D. (2021) Brain Function Network: Higher Order vs. More Discrimination. *Frontiers in Neuroscience*, **15**, Article ID: 696639. https://doi.org/10.3389/fnins.2021.696639

[18] Su, H., Zhang, L., Qiao, L. and Liu, M. (2022) Estimating High-Order Brain Functional Networks by Correlation-Preserving Embedding. *Medical & Biological Engineering & Computing*, **60**, 2813-2823. https://doi.org/10.1007/s11517-022-02628-7

[19] Biswal, B., Zerrin Yetkin, F., Haughton, V.M. and Hyde, J.S. (1995) Functional Connectivity in the Motor Cortex of Resting Human Brain Using Echoplanar MRI. *Magnetic Resonance in Medicine*, **34**, 537-541. https://doi.org/10.1002/mrm.1910340409

[20] Marrelec, G., Krainik, A., Duffau, H., P'el'egrini-Issac, M., Leh'ericy, S., Doyon, J. and Benali, H. (2006) Partial Correlation for Functional Brain Interactivity Investigation in Functional MRI. *Neuroimage*, **32**, 228-237. https://doi.org/10.1016/j.neuroimage.2005.12.057

[21] Lee, H., Lee, D.S., Kang, H., Kim, B.-N. and Chung, M.K. (2011) Sparse Brain Network Recovery under Compressed Sensing. *IEEE Transactions on Medical Imaging*, **30**, 1154-1165. https://doi.org/10.1109/TMI.2011.2140380

[22] Plis, S.M., Sui, J., Lane, T., Roy, S., Clark, V.P., Potluru, V.K., Huster, R.J., Michael, A., Sponheim, S.R., Weisend, M.P., *et al.*, (2014) Highorder Interactions Observed in Multi-Task Intrinsic Networks Are Dominant Indicators of Aberrant Brain Function in Schizophrenia. *NeuroImage*, **102**, 35-48. https://doi.org/10.1016/j.neuroimage.2013.07.041

[23] Chen, X., Zhang, H., Gao, Y., Wee, C.-Y., Li, G., Shen, D. and Initiative, A.D.N.

(2016) High-Order Resting-State Functional Connectivity Network for MCI Classification. *Human Brain Mapping*, **37**, 3282-3296. https://doi.org/10.1002/hbm.23240

[24] Liu, J., Ji, S. and Ye, J. (2012) Multi-Task Feature Learning via Efficient l2, 1-Norm Minimization.

[25] Guyon, I. and Elisseeff, A. (2003) An Introduction to Variable and Feature Selection. *Journal of Machine Learning Research*, **3**, 1157-1182.

[26] Szenkovits, A., Meszl'enyi, R., Buza, K., Gask'o, N., Lung, R.I. and Suciu, M. (2018) Feature Selection with a Genetic Algorithm for Classification of Brain Imaging Data. In: Stańczyk, U., Zielosko, B. and Jain, L.C., Eds., *Advances in Feature Selection for Data and Pattern Recognition*, Springer, Berlin, 185-202. https://doi.org/10.1007/978-3-319-67588-6_10

[27] Chang, C.-C. and Lin, C.-J. (2011) Libsvm: A Library for Support Vector Machines. *ACM Transactions on Intelligent Systems and Technology* (*TIST*), **2**, Article No. 27. https://doi.org/10.1145/1961189.1961199

[28] Dadi, K., Rahim, M., Abraham, A., Chyzhyk, D., Milham, M., Thirion, B., Varoquaux, G., Initiative, A.D.N., *et al.* (2019) Benchmarking Functional Connectome-Based Predictive Models for Resting-State fMRI. *NeuroImage*, **192**, 115-134. https://doi.org/10.1016/j.neuroimage.2019.02.062

[29] Sun, L. and Guo, T. (2020) Functional Brain Network Learning Based on Spatial Similarity for Brain Disorders Identification. *Journal of Applied Mathematics and Physics*, **8**, 2427-2437. https://doi.org/10.4236/jamp.2020.811179

[30] Xue, Y., Zhang, L., Qiao, L. and Shen, D. (2020) Estimating Sparse Functional Brain Networks with Spatial Constraints for MCI Identification. *PLOS ONE*, **15**, e0235039. https://doi.org/10.1371/journal.pone.0235039

[31] Ruan, Q., D'Onofrio, G., Sancarlo, D., Bao, Z., Greco, A. and Yu, Z. (2016) Potential Neuroimaging Biomarkers of Pathologic Brain Changes in Mild Cognitive Impairment and Alzheimer's Disease: A Systematic Review. *BMC Geriatrics*, **16**, Article No. 104. https://doi.org/10.1186/s12877-016-0281-7

[32] M'arquez, F. and Yassa, M.A. (2019) Neuroimaging Biomarkers for Alzheimer's Disease. *Molecular Neurodegeneration*, **14**, Article No. 21. https://doi.org/10.1186/s13024-019-0325-5

[33] Risacher, S.L. and Saykin, A.J. (2013) Neuroimaging and Other Biomarkers for Alzheimer's Disease: The Changing Landscape of Early Detection. *Annual Review of Clinical Psychology*, **9**, 621-648. https://doi.org/10.1146/annurev-clinpsy-050212-185535